Presented at the International Conference
on Metals Science; the Emerging Frontiers,
Varanasi, India, November 23 - 27, 1977

LBL-6998

CONF-771165--1

HIGH RESOLUTION AND HIGH VOLTAGE ELECTRON MICROSCOPY AT THE UNIVERSITY OF CALIFORNIA, BERKELEY

G. Thomas and K. H. Westmacott

January 1978

Prepared for the U. S. Department of Energy
under Contract W-7405-ENG-48

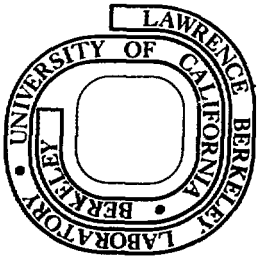

LBL-6998

Department [illegible] Materials [illegible]
Materials and [illegible]
University [illegible]

INTRODUCTION

[illegible]

field of materials [illegible] property relations. [illegible] to the atomic level [illegible] materials for specific [illegible] tinuously. These developments [illegible] specific applications rather [illegible] error[1]. Our [illegible] phenomena [illegible] and improvement [illegible] [illegible] between processing [illegible]

[illegible] available for [illegible] significantly. Thus, [illegible] characterize microstructures [illegible] requiring different modes of operation [illegible] being exploited [illegible] time consuming and difficult [illegible] with [illegible] 100 kV electron microscopes. Consequently, [illegible] of lattice imaging which were formerly [illegible] study [illegible]

large unit cell dimensions[2] are now being applied to metals and other materials of practical importance. Successful imaging of lattice planes in two crystal dimensions--the so-called structure imaging--has resulted in important new understanding of the structure of oxide crystals near the atomic level (see, e.g., Allpress and Sanders[3], Cowley and Iijima[4]) while the fringe imaging technique which resolves lattice planes in one dimension has provided a wealth of new quantitative information on layered structures (Amelinckx[5]) and on alloy systems of practical significance (Phillips[6]; Sinclair, Gronsky and Thomas[7]). These approaches lead us to the possibility of real space crystallography.

In other developments electron microscopes with accelerating voltages up to 3 MeV have become available, and this has expanded the range of materials that can be studied, and led to other unanticipated advantages (e.g. critical voltage effect, specimen environment control).

In addition to these changes in conventional fixed beam electron microscope usage the introduction of scanning transmission microscope has increased the scope for combined structural/analytical analysis and interesting results from these techniques are now being published. In the present paper, however, we consider only recent applications of high resolution and high voltage techniques at Berkeley using 100 kV conventional TEM's and a standard 650 kV high voltage electron microscope.

BASIC BACKGROUND

The information that is obtained by electron microscopy methods is derived from the scattering processes that take place when the electron beam travels through the specimen. There are two main types of scattering: (a) elastic--the interaction of the electron with the effective

potential field of the nuclei--involving no energy losses and which can be coherent or incoherent (poor phase relationships) and (b) inelastic--the interaction of the electron beam with the electrons in the specimen-involving energy losses, i.e., absorption. It is the elastic scattering that produces a diffraction pattern; and, if the scattering centers in the specimen are arrayed in an orderly regular manner such as in crystals, the scattering is coherent and results in spot patterns, Kikuchi patterns or, if the sample is a fine-grained polycrystal, ring patterns. Thus the information from electron microscopy includes morphology (images) structure (diffraction), and chemical analysis (spectroscopy) as indicate in Fig. 2. The electron microscope is truly a versatile instrument.

The basic reason for the utilization of the electron microscope is its superior resolution resulting from the very small wavelengths of electrons compared to other forms of radiation for which an optical system can be constructed. The resolution is given by the Rayleigh formula which is derived from considering the maximum angle of electron scattering (α) which can pass through the objective lens.

This formula is:

$$R = \frac{0.61\lambda}{\alpha} \qquad (1)$$

where R is the size of the resolved object, λ is wavelength, and α is identical to the effective aperture of the objective lens.

In the electron microscope the effective aperture is limited chiefly by spherical aberration. The spherical aberration error is:

$$\Delta S = C_s \alpha^3 \qquad (2)$$

where C_s is the coefficient of spherical aberration of the objective lens (≃ focal length, which is about 2mm or less in modern instruments).

Thus R increases with decreasing α; whereas ΔS decreases with decreasing α. As a result, in electron optics one arrives at an optimum aperture and minimum resolution given by:

$$\alpha_{opt} = A(\lambda^{1/4})C_s^{-1/4}, \tag{3}$$

$$\Delta R_{min} = B(\lambda^{3/4})\, C_s^{1/4} \tag{4}$$

where A, B are constants of order 1.

The wavelength of electrons depends on the accelerating voltage and is given by the DeBroglie equation modified by relativistic effects to be

$$\lambda = \frac{12.26}{E^{1/2}(1 + 0.9788 \times 10^{-6}E)^{1/2}} \text{ Å} \tag{5}$$

where E is the accelerating potential (volts); thus λ decreases with E. Some values pertinent to electron microscopy are given below.

E(volts)	λ(Å)	$\lambda^{-1}(Å)^{-1}$	$(v/c)^2$
100 kV	0.037	27.02	0.3005
500 kV	0.0142	70.36	0.7445
1MeV	0.0087	114.7	0.8856
10MeV	0.0012	846.8	0.9976

Another advantage of the small wavelength of electrons is that the depth of field and depth of focus are very large in electron microscopes.

At 100 kV the point resolution $\Delta R_{min} \simeq 3.5$Å for $C_s = 1.6$mm. Other factors which affect resolution are astigmatism and chromatic aberration of

the imaging system, and chromatic aberration resulting fron energy losses in the specimen. These errors produce poor resolution for non-axial illumination. However, since Cs decreases with voltage, in theory we should be able to attain point resolutions better than 2Å by raising the voltage to 0.5 MeV provided adequate electronic and mechanical stability is also achieved.

The conventional imaging mode for TEM is either bright field (transmitted electrons) or dark field (diffracted electrons). However, if the aperture of the objective lens is large enough to allow recombination of the transmitted and diffracted beams to occur a lattice image is obtained which is a magnified picture of the planes which are diffracting. At the present time the resolution for this mode of imaging is about 1.5Å. Applications of this method are discussed latter.

Unless one utilizes a very fine probe, as in STEM, then, because of spherical aberration, the error in selection of the area for diffraction analysis can be appreciable. The minimum selected area ΔA is given by Eq. (2), replacing α by the Bragg angle θ, i.e.,

$$\Delta A \simeq C_s\theta^3 \simeq C_s(\lambda/d)^3 \text{ for small angles.}$$

Since C_s varies approximately as λ^{-1} then ΔA varies as λ^2 and thus decreases rapidly with increasing voltage. For example for a fixed beam TEM, $\Delta A \simeq 2\mu m$ at 100 kV and $0.02\mu m$ at 1 MeV. This reduced selected area diffraction error illustrates another advantage of high voltage microscopy.

HIGH RESOLUTION ELECTRON MICROSCOPY

The resolution of presently available commercial transmission electron microscopes is limited to 3.5Å point-to-point and 2Å line. This limit is due to imperfections in the objective lens, and mechanical (specimen stage) and electronic (high voltage) instabilities in the instrument. Thus it is not yet possible to achieve atomic resolution and identification in close-packed structures such as metals, although many examples for complex oxides and minerals are now being obtained.

In a specially designed 500 kV instrument fitted with an objective pole piece of extremely low spherical aberration coefficient impressive demonstrations of atomic resolution in a metal has recently been published[8]. In the past few years research at the University of California at Berkeley has shown that considerable advances in studying near atomic scale structures and phenomena can be achieved with commercial 100 kV instruments using lattice fringe imaging, particularly when this is combined with laser optical diffraction techniques. These methods have proved to be far superior to conventional TEM in providing information not only on the detailed structural configuration of lattice planes, but also on local compositional changes. In this section, several examples of this work are given.

GRAIN BOUNDARY PRECIPITATION REACTIONS IN Al-Zn[9]

Application of the lattice fringe imaging technique to the study of grain boundary reactions in Al-Zn has revealed the detailed structure of the boundary regions as well as compositional changes up to 10Å from the boundary. Fig. 3 is a lattice image of a faceted region of a single boundary precipitate in an Al-30at%Zn alloy aged for 1 min at 135°C.

The fringes are continuous through both the precipitate and its facet, but careful measurements revealed that the spacing of the fringes within the facet were 1.6 ± 0.5% larger than those in the precipitate. This variation indicates that the facet region is enriched in Zn relative to the precipitate, and fine scale measurements revealed that a solute gradient exists away from the boundary interface in both the matrix and precipitate (See Fig. 4). The potential for establishing the role of grain boundaries in boundary-nucleated phase transformations by lattice imaging techniques is thus clearly demonstrated. Other studies at high magnification in this system have elucidated the nature of the precipitate-matrix interface and its dependence on orientation. Atomic spacing ledges have been observed (these are not resolved in conventional micrographs) and are thought to be important in the phase transformation mechanism.

LATTICE IMAGING OF GRAIN BOUNDARIES IN CERAMICS[10]

Grain boundaries have a special significance in ceramic materials since consolidation of the powder during material preparation and the resulting mechanical properties both depend on the atomic diffusion processes that occur in these regions. Consequently, the lattice fringe imaging technique is eminently suitable for studying these structures on an atomic scale. When hot-pressed MgO fluxed silicon nitride is heated above ~1000°C it is found that its strength and toughness drops dramatically. This decrease is generally attributed to the presence of a glassy intergranular phase, which at high temperatures rapidly decreases in viscosity with increasing temperature. However, no observations of a glassy phase had been made until the lattice imaging work of Clarke and Thomas[10] provided direct evidence for its existence. Very careful studies in which the diffraction conditions for high resolution fringe imaging on

both sides of a vertical grain boundary were simultaneously satisfied revealed remarkable grain boundary detail. Fig. 5 shows a striking example of the lattice plane structure in the vicinity of a triple boundary junction in Si_3N_4. An amorphous intergranular phase is clearly seen concentrated in this region as well as the sharp decrease in layer thickness further from the triple point. Studies of many such boundaries have shown that the glassy constituent is very heterogeneously distributed.

ELECTRON MICROSCOPY OF STEELS

Steels represent perhaps the most important class of materials as far as the national and international economies are concerned. A great challenge to the metallurgist is the economic production of better grades of steels having superior mechanical properties e.g. high strength with high toughness, good formability etc. Over the past 10-15 years we have been engaged in two major programs of steel alloy design a) high strength, tough structural steels, and b) high strength formable steels for better strength: weight properties e.g. for automobile applications (fuel savings).

a) High Strength, Tough Structural Steels

High strength structural steels are used extensively for components such as aircraft landing gear, missiles, rocket casings, armor plate and other defense applications. In addition, where such steels have high hardness and consequent abrasion resistance, they are used in mining operations (e.g., buckets, comminution, mineral processing operations). The limiting factor in the use of high strength steels is their toughness. In practice, toughness and ductility are required to resist crack propagation and ensure sufficient formability for successful fabrication of the steel into engineering components.

Most of the commercial high strength steels in use today are designed largely by trial and error methods, and almost all of them suffer from inadequate toughness at high strength levels.

Our program has been under way since 1964 and involves a systematic study of the relation between martensitic structures and properties utilizing a series of Fe/C/X experimental steels (X is the substitutional solute). The martensite transformation, if controlled such that the inhomogeneous shear component occurs by slip, not twinning, is the most efficient means of producing dense uniformly dislocated substructures--an essential component for strength and toughness[11]. The main factor controlling this aspect of the transformation is composition, especially per cent carbon [affects transformation temperature (M_S) and strength of the austenite] which must be controlled to maintain $M_S > 200°C$. In addition, we have found that stable retained austenite is beneficial to toughness[12]. Detailed TEM and sophisticated diffraction analyses of microstructures such as that shown in Fig. 6 and schematically in Fig. 7 have revealed that the microstructure which corresponds to optimum properties involves the following principal factors:

1. Production of dislocated packet martensite.
2. Surrounding of each martensite crystal in the packet by stable retained austenite.
3. Hardening of the steel to avoid upper bainite (or other undesirable transformation products).

The retained austenite has several beneficial aspects: it is itself ductile and therefore enhances toughness, e.g., by crack blunting, and it prevents brittle interlath carbide films from forming due to autotempering during the $\alpha \rightarrow$ martensite transformation.

The current program is aimed at optimizing these microstructural features by using minimal alloy contents. New steels based on Fe/Cr/C with Mn or Ni quaternary additions show better combinations of strength and toughness than any existing commercial steel[13]. These steels have strong potential for applications in the mining industry. Other properties of commercial interest including fatigue, corrosion behavior and wear resistance, are also being investigated.

b) Dual-Phase Steels for Improved Strength and Weight Applications

There is currently a need for higher strength steels with good formability dictated by today's energy and resource conservation requirements. These provide an interesting challenge to achieve weight reduction and fuel savings, as for example in the transportation industries.

To achieve these goals microstructural features were developed by using the principles of composites to obtain duplex ferrite-martensite (DFM) structures in low-carbon simple steels[14]. These two-phase steels contain controlled amounts of martensite (strong phase) in a ferrite martrix (soft phase), and are capable of optimizing the ever conflicting property requirements of strength and ductility, contingent upon a favorable choice of alloy composition and processing.

This composite system is of interest because the required duplex microstructure can be produced solely by utilizing solid state phase transformations without resorting to mechanical or thermomechanical treatments. The strengthening principle of the DFM structure involves the incorporation of inherently strong martensite as a load carrying constituent in a soft ferrite matrix. The latter then supplies the system with the essential element of ductility. This fiber loading concept contrasts markedly with microalloyed high strength low-alloy (HSLA) steels whose

principal strength is derived from grain refinement and precipitation of finely dispersed alloy carbides. A new DFM alloy, now patented by the U.S. Department of Energy, of composition Fe/2%Si/0.1%C, has been developed with silicon used to expand the two-phase ($\alpha + \gamma$) field and increase the flexibility for heat treatment. The tensile properties of these steels are superior to those of commercial HSLA steels. Moreover, they already exceed the industrial goal for HSLA steels for the automobile industry. The characteristics of DFM structure include: (a) an extremely high rate of work hardening in the early stage of plastic deformation, (b) a smooth transition from elastic to plastic deformation without showing yield point phenomena, and (c) high ratio of tensile/yield strength and good elongation to necking.

Important problems in characterising these alloys include studies of the α/martensite interface and estimating the carbon contents in the two phases. High resolution TEM lattice imaging has been successfully applied to these problems[15], and this is no easy task because of the added difficulties of astigmatism correction due to the magnetic properties of steel.

A typical example is given in Fig. 8. In Fig. 8(a) an area containing ferrite-martensite boundaries has been imaged under conventional B.F. conditions and it is evident that little structural detail of the interface is revealed. By contrast in Fig. 8(b) a {110}lattice fringe image is shown. Similar continuity of lattice fringes is clearly seen at the α/martensite boundary; the martensite region is distinguished by black and white patches probably due to the high density of dislocations. The continuity in this case is interpreted as follows. Assuming the K-S orientation relationship holds in the $\alpha+\gamma$ mixture at 950°C then for $(111)\gamma$ the particular variant of the six possible $\{110\}\alpha$ will be the $(101)\alpha$ which already exists parallel to $(111)\gamma$ across the original

$\gamma - \alpha$ interface. Hence on transformation $\gamma \rightarrow \alpha$, $(111)\gamma$ becomes $(101)\alpha$ parallel to $(101)\alpha$ in the pre-existing ferrite. This is consistent with the measured d spacings.

The principal difficulties encountered in imaging lattice fringes in martensitic steels are associated with (i) relatively small lattice spacings (largest d = 2.03Å), (ii) correction of objective astigmatism due to the magnetic field of the specimen, and (iii) very high, localized strain fields in the structure. We have demonstrated, however, that the lattice imaging technique can be successfully applied to the martensitic transformation in steels.

HIGH VOLTAGE MICROSCOPY

The present high voltage microscope facility at University of California, Berkeley consists of an Hitachi HU 650 installed in 1969 with a resolving power of ~20Å. Within the next two years, however, a new HVEM capable of achieving a resolution of 3.5Å point-to-point will be added at the Lawrence Berkeley Laboratory adjacent to the U.C. campus. With a maximum accelerating voltage of 1.5 MeV, this instrument will be the largest in the U.S. and as such will be made available to qualified users throughout the country, and of course from abroad.

From the discussion presented earlier the clear advantages of high voltage electron microscopy are (i) the increased penetration (ii) the reduction in spherical aberration and diffraction error (iii) the reduction in ionisation damage, and capability for in-situ knock-on damage studies, and (iv) the ability to control the specimen environment. The first three benefits are being exploited currently in research in materials science

at Berkeley, selected examples of which are given here, and a research program performed in cooperation with Prof. P. R. Swann's group at Imperial College, London will illustrate the importance of controlling the specimen environment in certain HVEM applications.

PHASE TRANSITIONS AND MAGNETIC PROPERTIES OF FERRITES

A program on ceramic magnets aimed at improving the magnetic properties of ferrimagnetic materials by controlling their microstructures is in progress at Berkeley. The studies emphasize the detailed characterization of microstructural features such as defects, second phases, etc. and the treatments necessary to introduce and eliminate these features. Among these studies of interest is the order $\rightleftarrows$ disorder transition in lithium ferrite[16]. In-situ experiments were done at Imperial College, London. The ordering reaction occurs near 750°C and the corresponding changes in microstructure were recorded dynamically using video methods*. Analysis of the results showed they were consistent with the theory of homogeneous nucleation and perfectly spherical growth. On the otherhand, the reverse disordering reaction appears to be initiated at the antiphase boundaries.

HIGH RESOLUTION STUDIES OF LATTICE DEFECTS: Weak Beam and Bright Field Methods

The importance of non-conventional techniques for improved imaging of defects has been recognised over the past decade. In particular the weak beam dark field imaging method[17] has found many champions. The image width of defects in contrast due to its strain field (i.e. when $\bar{g}.\bar{b} \neq 0$) depends on the extinction distance (ξg) approximately as $\xi g/3$. The extinction distance $\xi g = (\Delta K)^{-1}$ where ΔK is the separation of the branches of the dispersion surfaces corresponding to the reflection operating. Thus to decrease image width, we must decrease ξg, a) by increasing the deviation

* A 16mm sound movie of these processes was shown at the conference.

from the exact Bragg condition (make s large), b) by increasing ΔK (make $\vec{g}$ large). The latter case offers a bright field imaging method since at high voltages many Bloch waves are excited so that large interband transitions are effective (ΔK increases). Unfortunately, this method is not yet widely recognised although it was first shown[18-20] in 1972. In either method image widths of ~20Å can be achieved and both methods are limited by contrast (i.e. the value of s and ng can only be increased to certain limits).

The bright field imaging technique involves exciting a systematic row of low order reflections and tilting the crystal to satisfy $\vec{g} = n\vec{g}$, s = o condition where n is ≥ 3. The clear advantages of this technique are the less stringent requirement for specimen stage stability, since the bright field imaging requires much shorter exposure times, and the greater ease of setting up and focussing the specimen. An illustration of this technique is shown in Fig. 9. When alloys of Cu-Mn-Al are aged at 300°C and subsequently at 240°C spinodal decomposition occurs into a Cu_2MnAl rich phase and a Cu_3Al rich phase[21]. During coarsening, the coherency strain is generally relieved by the generation of $\frac{1}{2}a\langle 100\rangle$ dislocations at the particle-matrix interface. Hence, under appropriate g = <200> diffracting conditions each set of dislocations in the network disappears in turn. In Fig. 9(b) the network has been imaged in the HVEM in weak-beam dark field conditions and in 9(a) under g = 800 (s = 0) conditions. The diffraction contrast width is reduced in both cases, and the corresponding increase in resolution is clearly comparable.

PRECIPITATION IN Al-Si ALLOYS AND THE BEHAVIOR OF INTERFACIAL DISLOCATIONS UNDER ELECTRON IRRADIATION

Many of the materials used in nuclear reactor applications are used in conditions where two or more alloy phases are present, and, while a

great deal is known about the behavior of single phase metals under irradiation, far less is known about precipitate behavior. As part of a program to study changes in precipitate structure during irradiation, binary Al-base alloys are being examined during in-situ irradiation in the HVEM.

Al-Si is a simple eutectic alloy system with a maximum silicon solid solubility of ~1.6%Si. When alloys are quenched from the single phase region to room temperature and subsequently aged in the range 150-250°C, particles, which have been identified as pure silicon, precipitate from solution. These particles possess a variety of morphologies ranging from platelets on {111} planes to laths and needles which lie along <110> directions. During in-situ irradiation of alloys with compositions in the range 0.5 - 1.0%Si in the HVEM, it became apparent that the strong contrast associated with many of the precipitates arose from the presence of interfacial dislocations around the precipitate periphery. During irradiation the interfacial dislocations absorb point defects and climb away from the precipitate/matrix interface. This behavior is illustrated in Fig. 10 . The progressive growth of loops surrounding <110> needles and {111} platelets is seen as a function of irradiation time at a temperature of ~150°C. Eventually the loops interact and coalesce with other loops (See Fig.10). Identical loop growth rates were measured for loops nucleated in the matrix and for the pre-existing loops around the precipitates. From previous work it was anticipated that the loops were perfect prismatic interstitial loops. This was confirmed by determining the Burgers vector of the loops and performing the standard contrast analysis following irradiation, and also by making the analysis on the interfacial loops in an as-quenched and aged specimen using a Philips 301 electron microscope.

It is surprising that the analysis shows the loops to be interstitial in view of the fact that Si has a larger lattice parameter than Al and precipitation of Si will therefore expand the lattice. Under these circumstances vacancy loops would be expected to form. However, it has been suggested by Beller[22] that precipitation of Si in Al occurs only when accompanied by vacancies in the ratio of one vacancy to four silicon atoms. If this quasi-stoichiometric model is indeed correct, it is possible that precipitation of silicon under these circumstances leads to the development of tensile stresses in the surrounding matrix. Nucleation of interstitial peripheral loops would then be favored. The goal of this research is to introduce a fine distribution of precipitates with associated vacancy loops which will be regenerated as the loops climb away from the interface by vacancy absorption.

THE EFFECT OF OXIDE FILMS ON LOOP FORMATION IN Al-Mg

High voltage electron microscopes have been used extensively to simulate, with electron irradiation, the conditions that exist in the core of nuclear reactors. The ability to concentrate the electron beam into a small area, and observe directly the nucleation and growth of point-defect clusters has been used to good effect in studies of the radiation damage processes in both simple and practical engineering materials. Since the foil specimens used are of the order of 1μ thick, the potential for specimen contamination or changes in chemistry during heating in the microscope is high, and the question of specimen environment is clearly an important one. Preliminary studies of the effect of changing the condition of the specimen surface has confirmed this point[23]. Aluminum-11% magnesium foils

were prepared by electropolishing and allowed to oxidise in air either at room temperature or at 200°C. When these specimens were subsequently irradiated at 150°C in the HVEM, secondary defect structures developed which appeared to be similar to those observed in pure Al and other FCC metals (See Fig. 11a). During subsequent growth of the loops, however, it became apparent that the loops had nucleated very close to the foil surfaces since long half loops developed which grew rapidly in a direction parallel to the surface (Fig. 11b,c). The proximity of the loops to the surfaces is suggested by the observed anomolously broad dislocation contrast and was confirmed by stereomicroscopy. Eventually, with continued irradiation and heating an irregular hexagonal dislocation network developed. The results may be explained in terms of the presence of the oxide films. It is known that surface films of MgO form when Al-Mg alloys are oxidized, and since the lattice parameter of MgO is 3% greater than that of the matrix, the growing films produce tensile stresses in the underlying metal. The preferential formation of interstitial dislocation loops in these regions thus occurs to reduce the stresses.

Several conclusions may be drawn from this preliminary study:

(i) the condition of the foil surface can be important in radiation damage experiments, hence environmental control is needed for proper interpretation of experimental results,

(ii) the formation of near-surface dislocation structure in the presence of an oxide film has interesting implications for void formation in partially oxidised materials, and

(iii) the formation of dislocation loops in a stress field is relevant to the problem of irradiation creep. Thus, this single example

performed without an environmental cell indicates the potential for obtaining greater understanding of interfacial phenomena when closely controlled environmental conditions are used in HVEM studies.

POLYTYPISM IN Mg SIALON

A final example will illustrate the utility of combining high voltage electron microscopy with the lattice fringe imaging technique.

Extensive polytypism in which the variable unit cell dimension is determined by composition has been reported in a number of so called sialon ceramics. X-ray analysis suggests that the polytypes are based on the wurtzite structure only with a regular insertion of a cubic stacked layer to accommodate an excess of one atomic species. The periodicity of the cubic stacked layers then determines the composition and unit cell of the polytype. Direct imaging of periodicities in the close packed stacking enables regions of one polytype structure to be identified and disorders and intergrowths between two structures examined. In Fig. 12, 32Å periodicity in a grain of magnesium Sialon polytype structure has been imaged using the Hitachi

FUTURE DIRECTIONS

Although we are obtaining considerably more information from lattice images than from conventional micrographs there are still a number of problems preventing us from attaining our goal of atomic resolution and identification. The resolution of conventional 100 kV instruments is limited. The thickness of specimens for image interpretation in terms of projected change density must be less than 100Å, which is generally not possible for

many materials. Both these factors can be overcome by utilizing higher voltage, high resolution instruments. Voltage increase also improves the possibility of studying beam-sensitive materials such as polymers and biological specimens. The interpretation of high resolution images, particularly for the imperfect lattices which are often encountered in practical materials, requires more sophisticated theories than currently used. Image formation is still not experimentally routine and the output of lattice images is low when compared to conventional images. Again, this situation should improve with better instrumentation. Specimen stages for in-situ experiments (e.g., heating, cooling, environmental) are far below even lattice fringes resolution. It is to be expected that much more reliable conclusions can be drawn about materials behavior by actually observing reactions at the atomic level as they occur. Also, whilst point resolutions ~ 4Å are now available, spectroscopic data cannot yet be obtained at these levels of spacial resolution. Thus, chemical analysis lags behind imaging, although developments in STEM and energy loss spectroscopy promise well for the future.

One final point that must be considered is that there is a feeling of excitement in electron microscopy now that we are on the verge of atomic resolution. Further improvements in instrumentation, e.g., beam source lens aberrations, which will also yield higher diffraction and spectroscopic resolution, can in the final analysis lead to the ultimate goal, viz., atomic resolution and identification.

ACKNOWLEDGEMENTS

The authors thank Drs. D. R. Clarke, R. Gronsky, J. Y. Koo, R. Mishra, O. Van der Biest and T. M. Shaw for their contributions, enthusiasm and endeavors in making this program a success. Support for the programs from the Basic Energy Science Department of Energy and National Science Foundation is gratefully acknowledged and one of us (KHW) also thanks National Science Foundation for a travel grant to attend the conference.

REFERENCES

1. G. Thomas, Fundamental Aspects of Structural Alloy Design, pp. 331, R.I. Jaffee and B.A. Wilcox (Eds.), Plenum Publ. Corp. (1977)

2. J.W. Menter, Proc. Roy. Soc., A236, pp. 119 (1956)

3. J.G. Allpress and J.V. Sanders, J. Appl. Crystall., 6. pp. 165 (1973)

4. J.M. Cowley and S. Iijima, Electron Microscopy in Mineralogy, H.R. Wenk (Ed.), pp. 123, Springer-Verlag, Berlin (1976)

5. S. Amelinckx, J. Van Lunduyt, J.A. Kohn, W. Eckart, Mat. Res. Bull., 8, pp. 339 (1973)

6. V.A. Phillips, Acta Met., 21, pp. 219 (1973)

7. R. Sinclair, R. Gronsky and G. Thomas, Acta Met., 24, pp. 789 (1976)

8. H. Hashimoto, 34th Ann. Proc. EMSA (Miami), (1976)

9. R. Gronsky and G. Thomas, 35th Ann. Proc. EMSA (Boston), G.W. Bailey (Ed.), pp. 116 (1977)

10. D.R. Clarke and G. Thomas, J. Am. Ceram. Soc. (1977) in press

11. G. Thomas, Iron and Steel Internat., 46, pp. 451 (1973)

12. J. McMahon and G. Thomas, Proc. 3rd Int. Conf. on Strength of Metals, Cambridge, 1, pp. 180, Inst. of Metals, London (1973)

13. M.F. Carlson, B.V.N. Rao, R.O. Ritchie and G. Thomas, 4th Int. Conf. on the Strength of Metals and Alloys, Nancy, France, pp. 509 (1976)

14. J.Y. Koo and G. Thomas, Met. Trans., 8A, pp. 525 (1977)

15. J.Y. Koo and G. Thomas, 35th Ann. Proc. EMSA (Boston), G.W. Bailey (Ed.), pp. 118 (1977)

16. O. Van der Biest, E.P. Butler and G. Thomas, 33rd Ann. Proc. EMSA (Las Vegas), G.W. Bailey (Ed.), pp. 36 (1975)

17. D.J.H. Cockayne, J. of Microscopy, 98, Pt. 2, pp. 116 (1973)

18. W.L. Bell and G. Thomas, Electron Microscopy and Structure of Materials, Univ. of Calif. Press, pp. 23 (1972)

19. R. Osieki and G. Thomas, 29th Ann. Proc. EMSA, pp. 178, Claitors, Baton Rouge (1971)

20. M.J. Goringe, E.A. Hewat, C. Humphreys and G. Thomas, Proc. 5th Europ. Congress on E.M., pp. 538, Inst. Phys., London (1972)

21. M. Bouchard and G. Thomas, Acta Met., 23, pp. 1485 (1975)

22. M. Beller, Z. Metallkde, 63, pp. 663 (1972)

23. K.H. Westmacott, 35th Ann. Proc. EMSA (Boston), pp. 51 (1977)

FIGURE CAPTIONS

Fig. 1. Scheme showing inter-relationship between various aspects of the alloy design program.

Fig. 2. Schematic diagram illustrating the information obtainable in a transmission electron microscope.

Fig. 3. Lattice image of a grain boundary precipitate in Al-30at%Zn showing a facet region within the precipitate. Quantitative measurements indicate changes in Zn enrichment within this region.

Fig. 4. Plot of {111} fringe spacing vs. distance across a grain boundary in an Al-9.5at%Zn alloy aged 30 min. at 180°C. Each measurement included 10 fringes (error bar shown on first point).

Fig. 5. High Resolution fringe imaging of adjacent grains in Si_3N_4 showing presence of glassy phase at the triple junction.

Fig. 6. (a) and (b) BF and DF showing thin continuous films of inter-lath retained austenite. $(200)_\gamma$ reflection shown in (c) is used for the DF, (c) SAD pattern showing the K-S orientation relationship between retained austenite and dislocated lath martensite.

Fig. 7. Schematic diagram of desirable microstructures for high strength, tough steels.

Fig. 8. The microstructure at martensite-ferrite boundaries in a duplex low carbon steel; (a) is a conventional BF micrograph of the boundary, (b) shows (110) lattice fringes from which boundary structure and composition can be found.

Fig. 9. Micrographs of interfacial dislocation networks in a Cu-Mn-Al alloy taken on a high voltage electron microscope under (a) high order bright-field, and (b) weak beam dark field, imaging conditions.

(c) shows the diffraction pattern with matrix and superlattice spots taken from same area.

Fig. 10. Sequence of micrographs showing the climb of precipitate-matrix interfacial dislocation loops in Al-1% Si during irradiation in the HVEM at 150°C.

Fig. 11. Sequence of micrographs showing the development of near-surface dislocation loop structure and networks in oxidised Al-11%Mg irradiated in the HVEM at 180°C (Courtesy Claitor Press, Baton Rouge).

Fig. 12. Lattice fringe image from a polytype of MgSiALON showing 32 Å fringe periodicity. The irregularities in the fringe spacings are due to disorder in the polytype structure. 650kV

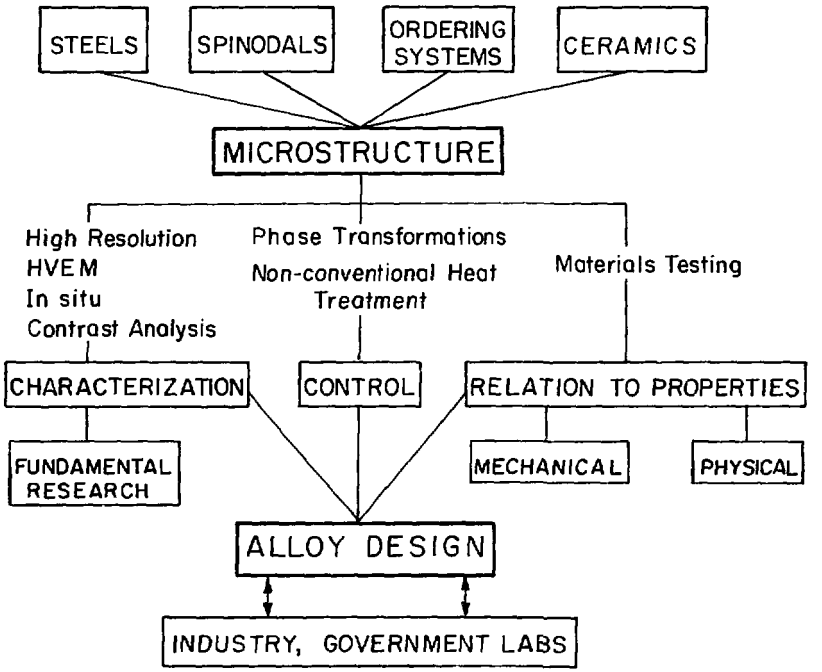
STEELS
SPINODALS
ORDERING SYSTEMS
CERAMICS
MICROSTRUCTURE
High Resolution
HVEM
In situ
Contrast Analysis
Phase Transformations
Non-conventional Heat Treatment
Materials Testing
CHARACTERIZATION
CONTROL
RELATION TO PROPERTIES
FUNDAMENTAL RESEARCH
MECHANICAL
PHYSICAL
ALLOY DESIGN
INDUSTRY, GOVERNMENT LABS
XBL761-6298

Fig. 1

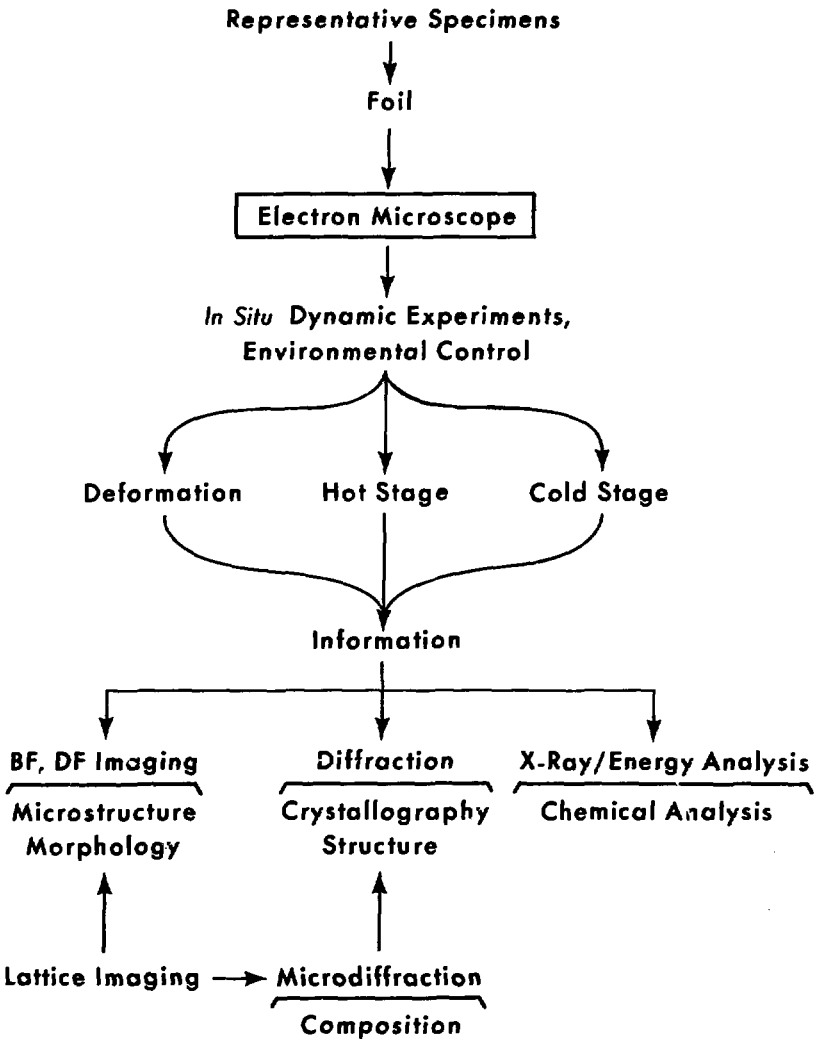
Representative Specimens
Foil
Electron Microscope
In Situ Dynamic Experiments,
Environmental Control
Deformation
Hot Stage
Cold Stage
Information
BF, DF Imaging
Microstructure
Morphology
Diffraction
Crystallography
Structure
X-Ray/Energy Analysis
Chemical Analysis
Lattice Imaging
Microdiffraction
Composition
XBL 7612-11183

Fig. 2

XBB 770-10526

Fig. 3

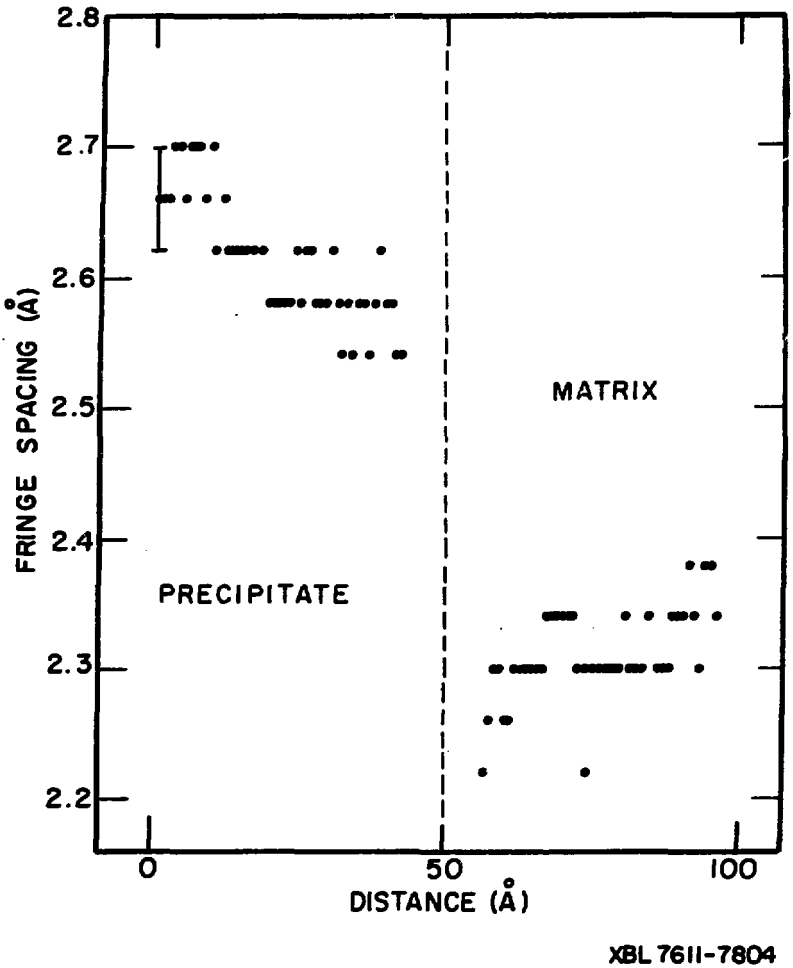
2.8
2.7
2.6
2.5
2.4
2.3
2.2
FRINGE SPACING (Å)
PRECIPITATE
MATRIX
0
50
100
DISTANCE (Å)
XBL 7611-7804

Fig. 4

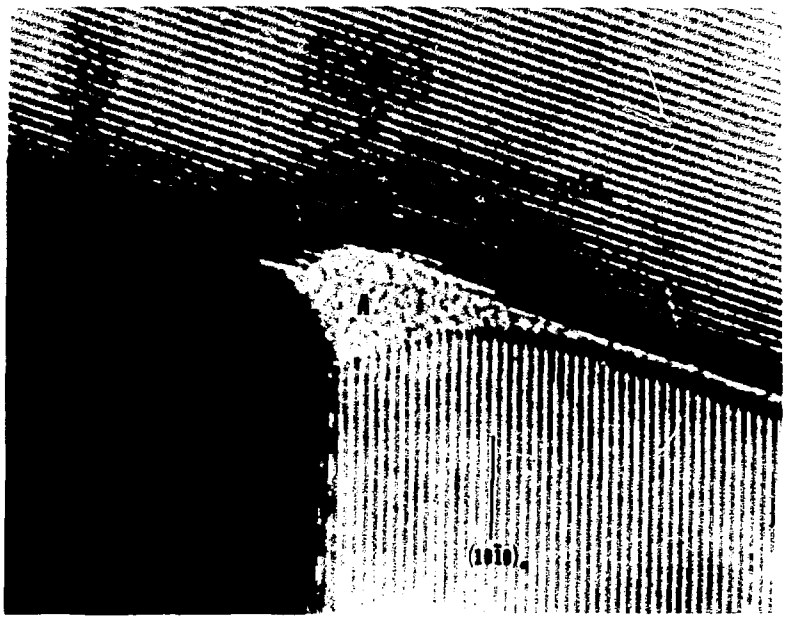

XBB 769-8516

Fig. 5

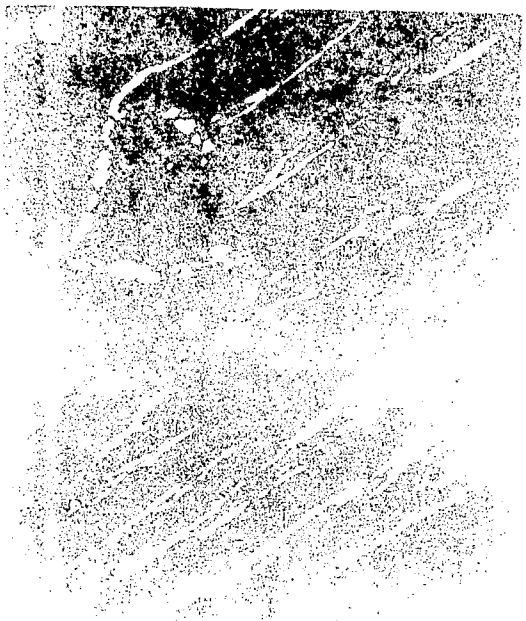

XBL 7711-10457

Fig. 7

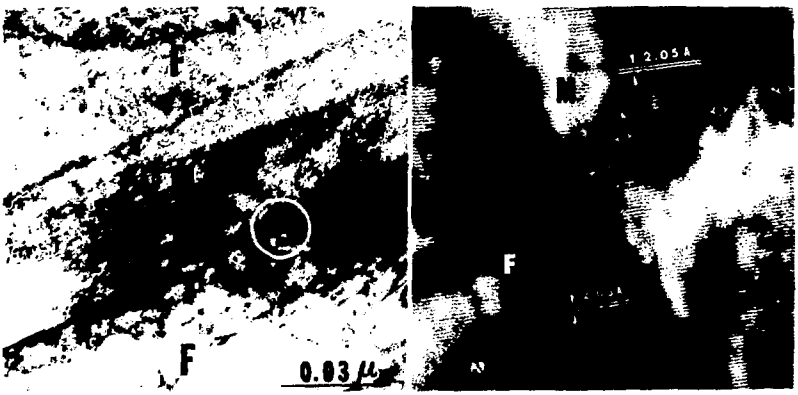

XBB 773-2297

8(a) 8(b)

Fig. 8

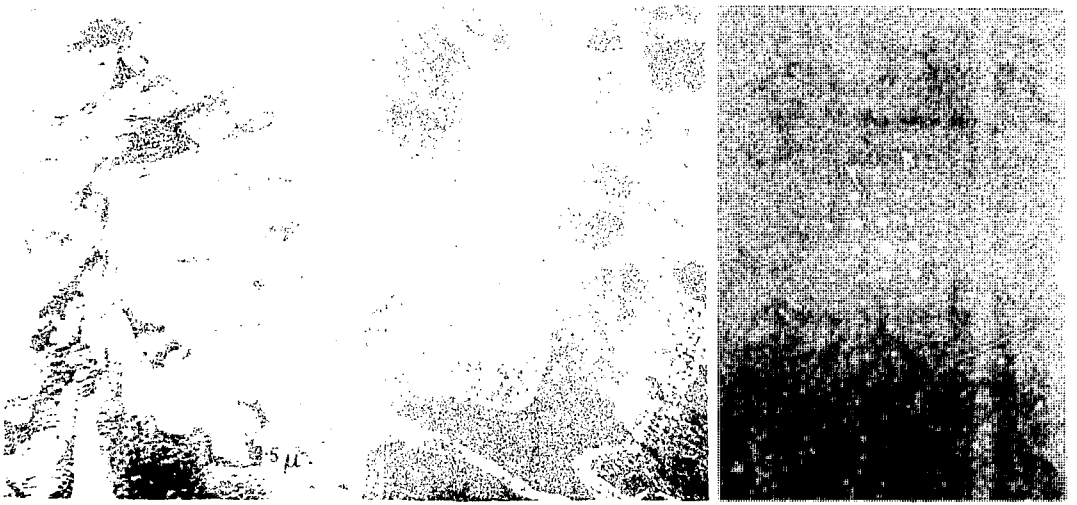
2.5 μ


t 9 min

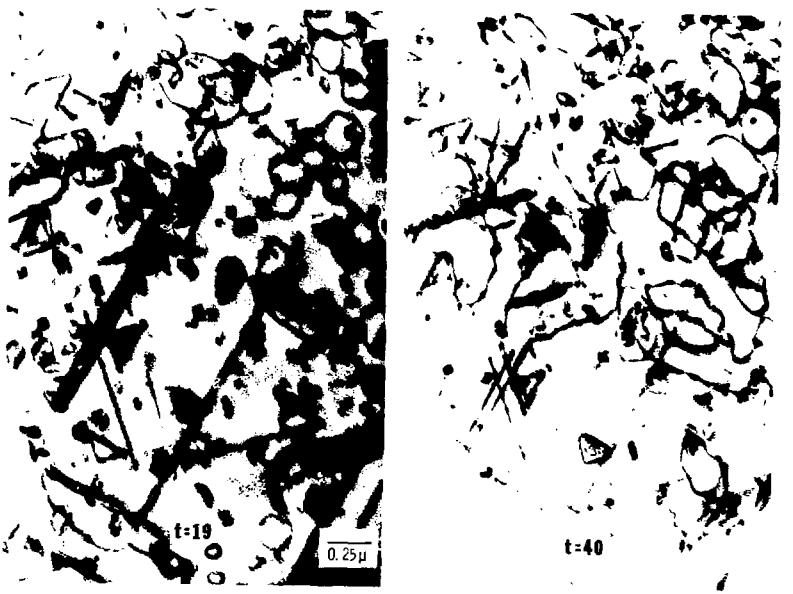

XBB 771-583

Fig. 10(b)

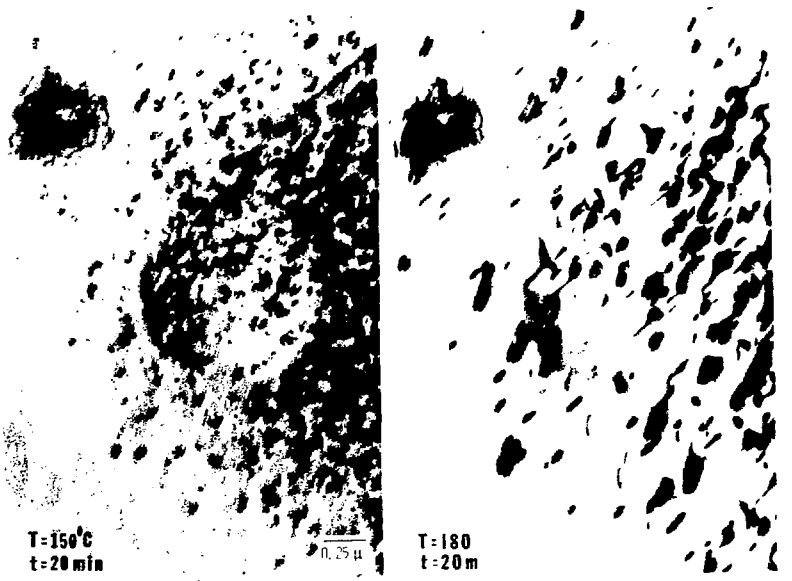

XBB 771-577

Fig. 11(a)

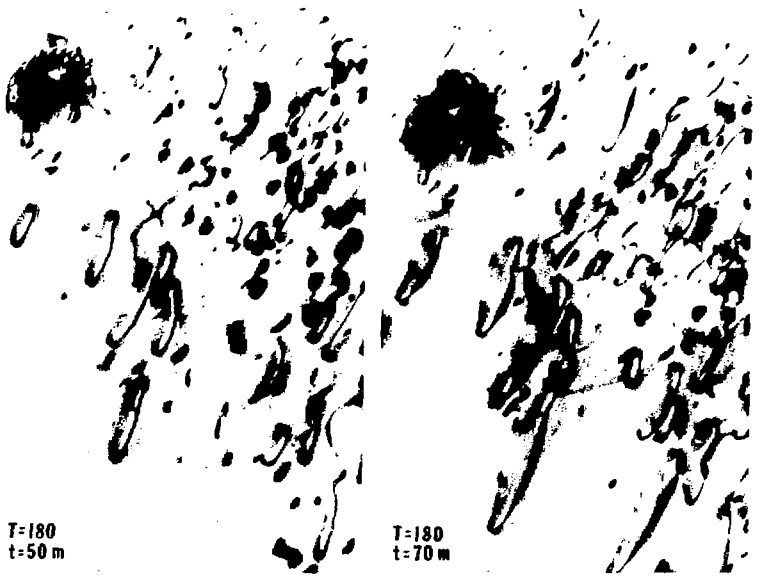

XBB 771-579

Fig. 11(b)

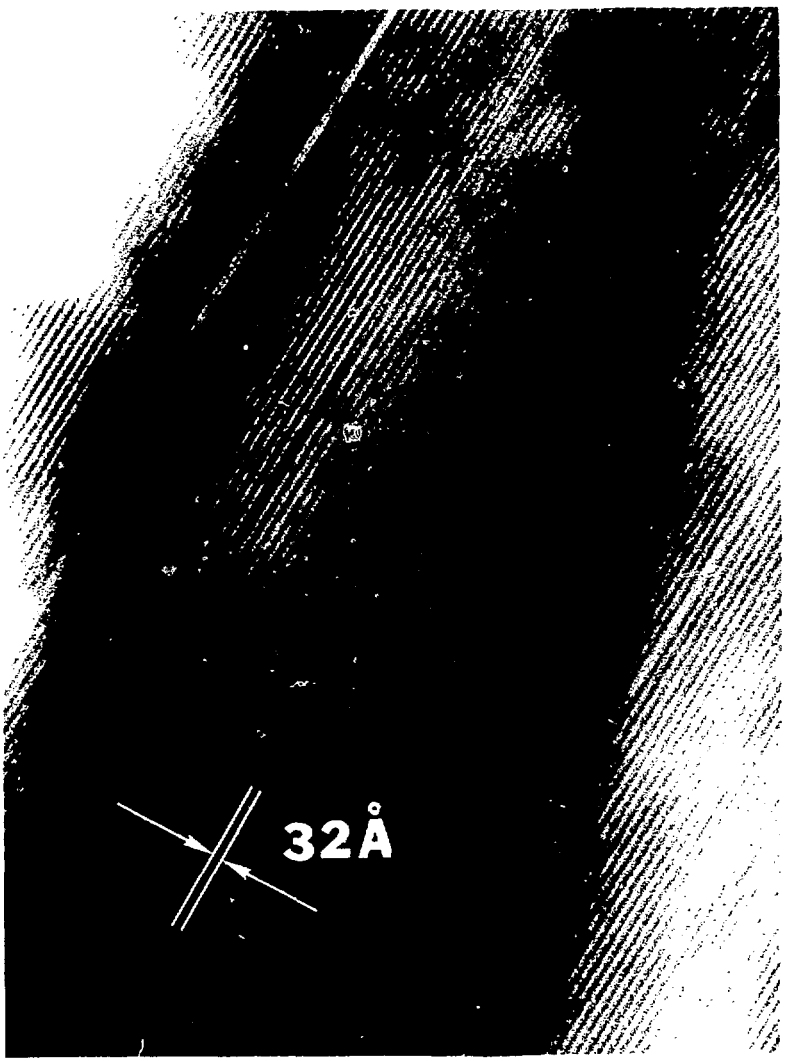

XBB 778-7955

Fig. 12